PAPER

Check for updates

Gradient copolymer prepared from alternating ring-opening metathesis of three monomers†

Francis O. Boadi [ID] and Nicole S. Sampson [ID] *

Bicyclo[4.2.0]oct-6-ene-7-carboxamide is a simple but highly strained olefin monomer which forms an alternating copolymer with cyclohexene in the presence of N-heterocyclic carbene-ruthenium catalyst. [4.2.0] moieties with a bulky substituent on C7 that chelate with the ruthenium center of the catalyst propagate more slowly than monomers that cannot chelate. Accordingly, the reactivity ratio of N-propylbicyclo[4.2.0]oct-6-ene-7-carboxamide with cyclohexene is significantly higher than that of N-(2-(2-ethoxyethoxy)ethan)-bicyclo[4.2.0]oct-6-ene-7-carboxamide with cyclohexene. A copolymerization involving the three monomers in a 1 : 1 : 2 (propyl : ethylene glycol : cyclohexene) molar ratio formed a gradient copolymer in a one-pot reaction. Surface hydrophobicity, topology, and thermal properties of the gradient copolymer were similar to those of a copolymer comprised of six microblocks prepared through multistep synthesis by alternately employing the same two bicyclo[4.2.0]oct-6-ene-7-carboxamides in each microblock. The properties of the gradient copolymer were distinct from a copolymer comprised of two larger blocks based on the same bicyclo[4.2.0]oct-6-ene-7-carboxamides.
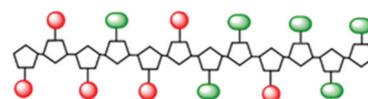
Introduction

Polymers containing more than one monomer (thus copolymers) are useful because their properties and functions may be tuned by varying comonomer compositions and sequence. Compositional variation of monomers, whether continuous (gradient) or discontinuous (block), along polymer chains, can influence the thermal,[1] mechanical,[2] surface,[3] and interfacial behaviors of copolymers.[4] Almost all gradient copolymers (GCPs) synthesized to date are two-monomer component systems. Even with only two monomers, gradient copolymers are useful and sometimes have properties superior to block copolymers. For example, when used as an additive in a polymer blend, gradient copolymers tend to decrease domain sizes; thus GCPs are suitable as reinforcing agents and blend compatibilizers.[5] In addition, GCPs usually have broad glass transition temperatures[2,6] and are attractive for applications such as pressure sensitive adhesives.

Numerous non-templated "living" polymerization techniques such as reversible addition–fragmentation chain transfer (RAFT),[7] atom transfer radical polymerization (ATRP),[8] nitroxide-mediated radical polymerization (NMRP)[5] and ring opening polymerization (ROP)[9] are popularly used in gradient polymer synthesis. Although ring opening metathesis polymer-
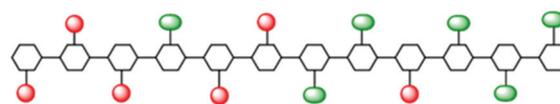
ization (ROMP) possesses a living character[10] and allows for tolerance of a wide range of functional groups,[11] its use in gradient copolymer synthesis is underexploited. The first ROMP gradient copolymer was reported in 2004 by Nguyen *et al.*[12] To control reactivities, they used two norbornene monomers whose substituents differed by their steric bulk. Since then, only a few other reports on GCP preparation have been issued, with all copolymers based on norbornene (Fig. 1).[13–16] Our lab-

Fig. 1 (A) typical ROMP gradient copolymer bearing cyclopentanyl backbone with a 2-carbon spacer, (B) AROMP gradient copolymer bearing cyclohexanyl backbone with a 6-carbon spacer (black line).

Department of Chemistry, Stony Brook University, Stony Brook, New York 11794-3400, USA. E-mail: Nicole.sampson@stonybrook.edu
†Electronic supplementary information (ESI) available: Spectral characterization data and kinetic data. See DOI: 10.1039/d1py00690h

oratory has shown that three cyclic olefin monomers can be used to prepare AB alternating copolymers *via* alternating ring-opening polymerization (AROMP) with specific sequences of different A-type monomers and provided evidence that sequence control modulates behavior.[3] Alternating copolymers were made by stepwise addition of the relevant number of equivalents of each monomer, a labor intensive and iterative process. Thus, we were motivated to develop gradient copolymerization with AROMP. Gradient copolymerization relies on different reactivities of monomer species.[12,14,17] In developing sequence controlled alternating copolymers, we had observed that bicyclo[4.2.0]oct-6-ene-7-carboxamide moieties with propyl side chain (**1a**) have marginally faster reactivity with cyclohexene (**2**) than glycine 7-substituted carboxamides.[3] Thus, the reactivities were insufficiently different and their copolymerization would result in a predominantly random copolymer. However, olefins substituted with chelating ligands can coordinate with ruthenium catalyst and impose steric constraints on an approaching monomer,[13] thus rendering them slower to propagate.

We reasoned that the reactivity of an "ethylene glycol" side chain would have further reduced reactivity compared to a glycine side chain because of the longer side chain and possibly strong chelating property of the glycol side chain (**1b**, Chart 1). Therefore, we hypothesized that the combination of **1a-*alt*-2**, **1b**, and **2** would yield a gradient copolymer in which the compositions **1a-*alt*-2** and **1b-*alt*-2** vary continuously along the chains. Herein, we employed bicyclo[4.2.0]oct-6-ene-7-carboxamides **1a** and **1b** and examined their reactivities with cyclohexene **2**. We prepared uniform, diblock, hexablock, and gradient copolymers (Fig. 2). Uniform copolymers are the copolymers consisting of only **1a-*alt*-2** (**P1**) or **1b-*alt*-2** (**P2**) strands while diblock, hexablock and gradient copolymers are made up of both **1a-*alt*-2** and **1b-*alt*-2** strands. Topological and thermal analyses of the copolymers revealed the dependence of functional properties on the length and location of (**1a-*alt*-2**) and (**1b-*alt*-2**) sequences within the copolymer chains. To the best of our knowledge, this is the first report of a ROMP gradient copolymer which does not rely on norbornene monomers. Importantly, the inclusion of monomer **2** introduces a larger spacer between the side chains (Fig. 1) offering entry to a more flexible copolymer.
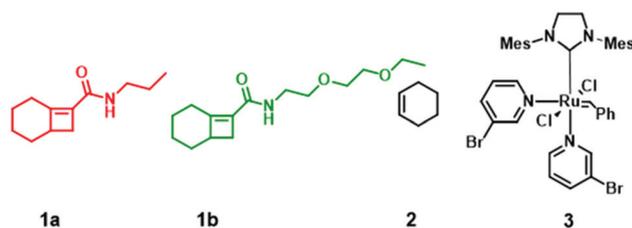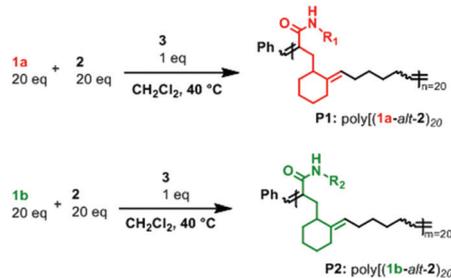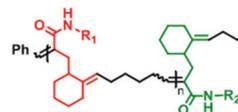

Chart 1 Monomers used for gradient copolymer synthesis. **1** and **2** react to form alternating strand poly(**1-*alt*-2**). All metathesis polymerization reactions were afforded by catalyst **3**.
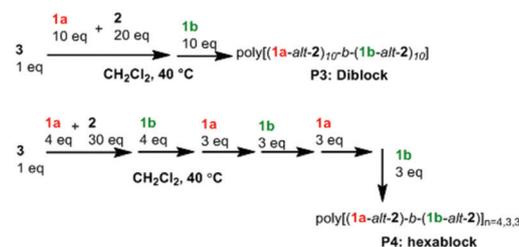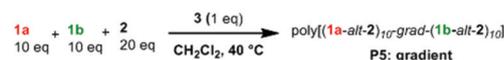

Fig. 2 Synthesis of (A) uniform AROMP copolymers from monomers **1** and **2** to form **P1**, poly(**1a-*alt*-2**)$_{20}$ or, **P2**, poly(**1b-*alt*-2**)$_{20}$ and, (B) sequence-defined AROMP copolymers from **1a**, **1b**, and **2** in (i) multiple steps to from diblock copolymer **P3** or hexablock copolymer **P4**, (ii) one-pot to yield gradient copolymer **P5** poly(**1-*alt*-2**)$_{10}$-*g*-poly(**1b-*alt*-2**)$_{10}$.

Results and discussion

N-Propylbicyclo[4.2.0]oct-6-ene-7-carboxamide **1a** was synthesized by coupling bicyclo[4.2.0]oct-6-ene-7-carboxylic acid and *N*-propylamine according to literature procedure (Fig. S1†)[18] and the ethylene glycol bicyclo[4.2.0]oct-6-ene-7-carboxamide monomer **1b** was similarly prepared by coupling bicyclo[4.2.0]oct-6-ene-7-carboxylic acid and *N*-2-(2-ethoxyethoxy)ethan-1-amine (Fig. S2†).

To demonstrate the impact of copolymer sequence on material properties such as topological and thermal behaviors, we synthesized uniform copolymers (**P1** and **P2**) whereby **P1** is made up of polymer chains containing only **1a-*alt*-2** units, **P2** consists solely of **1b-*alt*-2** units, and diblock (**P3**), hexablock (**P4**), and gradient (**P5**) are copolymers of **1a**, **1b**, and **2**. The reactivity ratios of **1a** & **1b** require that **P3** and **P4** be synthesized by multi-step AROMP (Fig. 2B). In contrast, **P5** was prepared in one step. All the polymers synthesized, **P1**–**P5**,

were characterized by ¹H-NMR spectroscopy (Fig. S3–S7†). Their molecular weights (MWs) and degree of polymerization (DP) were determined by gel permeation chromatography (GPC) and ¹H-NMR spectroscopy, respectively. As determined by GPC, the polymers exhibited a unimodal distribution (Fig. S8†) and MW dispersities ($Đ_M$) were narrow with $Đ_M$ = 1.2–1.5 (Table 1). The theoretical molecular weights of the polymers match the molecular weights determined by DP analysis. However, molecular weights determined by polystyrene standard calibration were different from the theoretical MW, most likely due to the difference in hydrodynamic volumes of the polymers described here compared with the polystyrene standards.[19] With polymer **P1**, 100% monomer conversion was achieved in less than 1.5 hours due to the higher reactivity of propyl[4.2.0]-based monomer with cyclohexene. In contrast for polymer **P2**, the ethylene glycol [4.2.0]-based monomer required twice the reaction time. The diblock copolymer **P3** was prepared in two steps by sequential addition. First, (**1a**-*alt*-**2**)₁₀ block was prepared using a twofold molar excess of cyclohexene. The second block (**1b**-*alt*-**2**)₁₀ was successfully installed by adding **1b** monomer to the reaction mixture containing poly(**1a**-*alt*-**2**)₁₀-with a living Ru-carbene and excess cyclohexene.

Full consumption of the [4.2.0]-based monomers **1a** and **1b** was confirmed by disappearance of protons between δ 2.6–3.0 ppm in the ¹H NMR spectra (Fig. 3A). Successful installation of the two blocks is also confirmed by GPC (Fig. 3B). The preparation of hexablock copolymer **P4**, was afforded by six sequential addition steps. Microblocks (**1a**-*alt*-**2**)₄-*b*-(**1b**-*alt*-**2**)₄-*b*-(**1a**-*alt*-**2**)₃ were fully installed in steps 1 through 3. However due to the slower reactivity of **1b**, steps 4–6 suffered from partial incorporation (Fig. S9†) which may result in reduced "blockiness" of the second half of the hexablock copolymers. Approximately 80% overall conversion was achieved for steps 1–6. Hence, a (**1**-*alt*-**2**) 16-mer with less than 50% incorporation of the **1b**-*alt*-**2** repeat (Table 1) was obtained. For gradient copolymer **P5**, full incorporation of both monomers **1a** and **1b** was achieved.

Ring opening kinetics

To determine the reactivity ratios of **1a**-*alt*-**2** and **1b**-*alt*-**2**, we examined ring opening metathesis (ROM) of **1a** and **1b** (Fig. 4A, Fig. S10–13†). Either **1a** or **1b** solution was treated
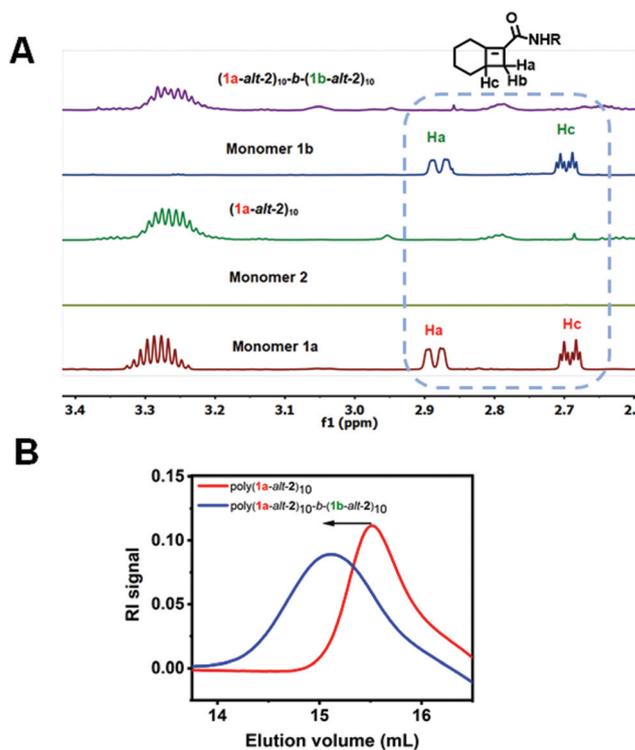

Fig. 3 Diblock copolymer **P3** was successfully prepared in two steps. In step 1, monomer **1a** was fully incorporated to form the first block, and monomer **1b** was fully incorporated at step 2 to install the second block as shown by both the ¹H-NMR overlay (A) and GPC chromatogram (B).

with a equimolar amount of **3**. Evidence of ROM was confirmed by the disappearance of Ru-styrenylidene proton (¹H NMR δ 19.17) (Fig. S12 & S13†). ROM of both **1a** and **1b** followed second-order reaction kinetics and **1a** reacted approximately three-fold faster than **1b** with catalyst **3** ($t_{1/2}$ = 21 min and 60 min respectively [**1**]₀ = [**3**]₀ = 0.15 M). The slower reactivity of **1b** with [Ru]-alkylidene is most likely due to the sterically bulky side chain.

Gradient copolymer kinetics

The incorporation of **1a** with respect to **2** and **1b** with respect to **2**, was assessed by ¹H-NMR spectroscopy at regular time

Table 1 Molecular weights and weight distribution ($Đ_M$) of copolymers[a]

Polymer	Type	[**1a**]:[**1b**]:[**2**]:[**3**]	Time (min)	DP[b]	**1b**-*alt*-**2**[c]	$M_{n,\text{theo}}$[d] (kDa)	M_n[f] (kDa)	$Đ_M$[e]
P1	Uniform	20:0:20:1	80	20	0.0	5.5	5.5	1.2
P2	Uniform	0:20:20:1	180	19	1.0	7.0	6.6	1.3
P3	2 Blocks	10:10:25[g]:1	180	19	0.5	6.3	6.0	1.5
P4	6 Blocks	10:10:30[g]:1	180	16	0.4	6.3	4.9	1.3
P5	Gradient	10:10:20:1	180	20	0.5	6.3	6.3	1.4

[a] Polymers were prepared with catalyst **3** (10 mM) at 40 °C in CH₂Cl₂. [b] DP refers to the total number of alternating -AB-pairs in the polymer; DP was determined by ¹H NMR spectroscopy integrating polymer against the end group phenyl (2H). [c] Mole fraction of **1b**-*alt*-**2** strand in the copolymers determined by ¹H NMR spectroscopy. [d] Theoretical molecular weight calculated based on total molar feed. [e] Molecular weight dispersity determined by GPC with polystyrene calibration. [f] Number average molecular weight (M_n) determined based on DP and percent composition of **1a**-*alt*-**2** and **1b**-*alt*-**2** strands in the copolymers. [g] Synthesis of **P3** & **P4** involved multiple steps and an excess of **2** was used to increase the reaction rate.
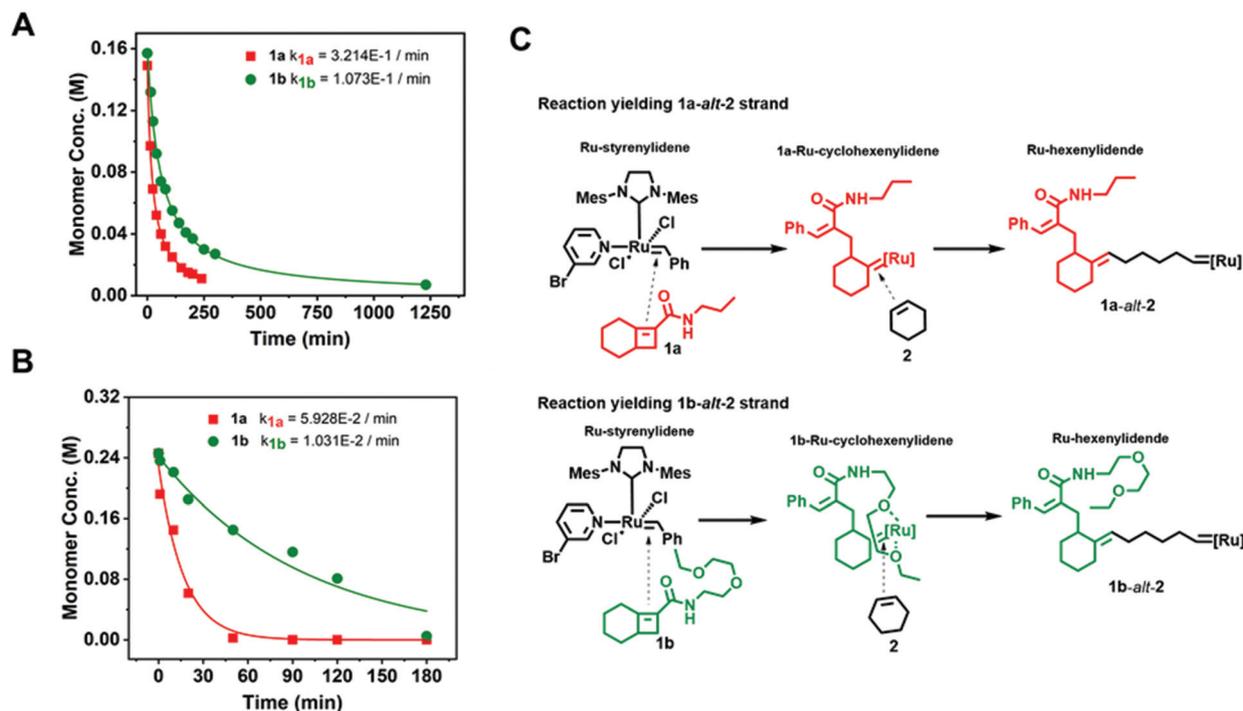
Fig. 4 The substituent on monomer **1** influences the rate of reaction of single monomer ring-opening metathesis (ROM) and of gradient copolymerization. (A) ROM reactions run with a single monomer **1**: [**1a**] = [**3**] = 0.15 M, or [**1b**] = [**3**] = 0.155 M. (B) Rate of disappearance of each **1** monomer in a gradient copolymerization of a mixture of **1a**, **1b**, and **2** at [**1a**] = 0.25 M, [**1b**] = 0.25 M, [**2**] = 0.49 M, [**3**] = 0.025 M. (C) ROM and AROM reactions of **1a** and **1b** with **2** and proposed orientation of alkylidenes and monomers that contribute to rate differences.

intervals for the copolymerization of **1a**:**2**:**1b** (1:2:1 molar ratio) (Fig. 4B). The reaction kinetics of **1a** or **1b** disappearance in the gradient copolymerization follow first order kinetics. In the gradient copolymerization, the rate of incorporation of **1a** is about 6 times faster than **1b** (half-lives $t_{1/2}$ (**1a**), $t_{1/2}$ (**1b**) ≈ 12 and 67 min respectively). The difference in rate of disappearance of **1a** and **1b** in the gradient copolymerization is larger than in the ROM reaction which suggests longer range effects on the addition to Ru-species occur. We also determined the relative reactivity ratios ($r_{\text{1a \& 2}}$, $r_{\text{1b \& 2}}$) for **1a** & **2** and **1b** & **2** respectively. Reactivity ratio is defined as the tendency for the propagating species to react with the same monomer over the other. To determine the reactivity ratios, we used the extended Kelen–Tüdös model (Fig. 5)[20] by analyzing the reaction mixture at moderate conversion (~40%) with feed ratios of monomers **1** varying from 0.1–0.9 equivalents (for **1a**), 0.9–0.1 equivalents (for **1b**), with one equivalent of monomer **2** (Tables S1 & S2†). The calculated relative reactivity ratios were $r_{\text{1a \& 2}}$ (2.17) and $r_{\text{1b \& 2}}$ (0.36). Data when fitted with the Jaacks model also gave similar reactivity ratios (Fig. S14†). The product of the reactivity ratios, $r_{\text{1a \& 2}} \cdot r_{\text{1b \& 2}}$ = 0.78 and indicates a nonideal copolymerization character, that is not exclusive or random, and thus a gradient copolymerization. The reactivity ratios suggest a potential medium gradient copolymer formation.[21]

Copolymer microstructure

The probabilities of finding certain sequences ($N(x)$) where x is the length of the sequence and μ is the mean sequence length are absolutely critical to make a more accurate prediction of compositional gradient heterogeneity in a copolymer.[22] To confirm that the molar combination of monomers **1a**, **2**, and **1b** (1:2:1) yields copolymer with gradient microstructure, $N(x)$ and μ were calculated (see ESI Table S3†). N**1a**-***alt***-**2** (1) = 0.32 and N**1b**-***alt***-**2**(1) = 0.74 are the probabilities of finding a sequence of a unit length, for (**1a**-***alt***-**2**)₁ and (**1b**-***alt***-**2**)₁; whereas the probabilities of finding a sequence of 3 unit lengths, (**1a**-***alt***-**2**)₃ and (**1b**-***alt***-**2**)₃, are N**1a**-***alt***-**2**(3) = 0.15, N**1b**-***alt***-**2**(3) = 0.05 respectively (Table S3, Fig. S15†). These imply there is a greater propensity of forming longer units of (**1a**-***alt***-**2**)$_{n≥3}$ at early stages of polymerization. Longer sequences of (**1b**-***alt***-**2**)$_{n≥3}$ are incorporated when **1a** monomer is significantly depleted (thus at later stages of polymerization). In addition, the mean sequence lengths were 3 and 1 for **1a**-***alt***-**2** and **1b**-***alt***-**2** respectively. Moreover, following the kinetics of polymerization to form **P5** with a molar feed ratio of 1:1:2 (**1a**, **1b**, **2**) by ¹H NMR spectroscopy (Fig. S16†) revealed formation of gradient copolymer. In this experiment, aliquots of polymer were taken from the reaction vial at different time points (10, 20, 50, 90, 120, and 180 min), quenched with ethyl vinyl ether, precipitated with diethyl ether, and dried under
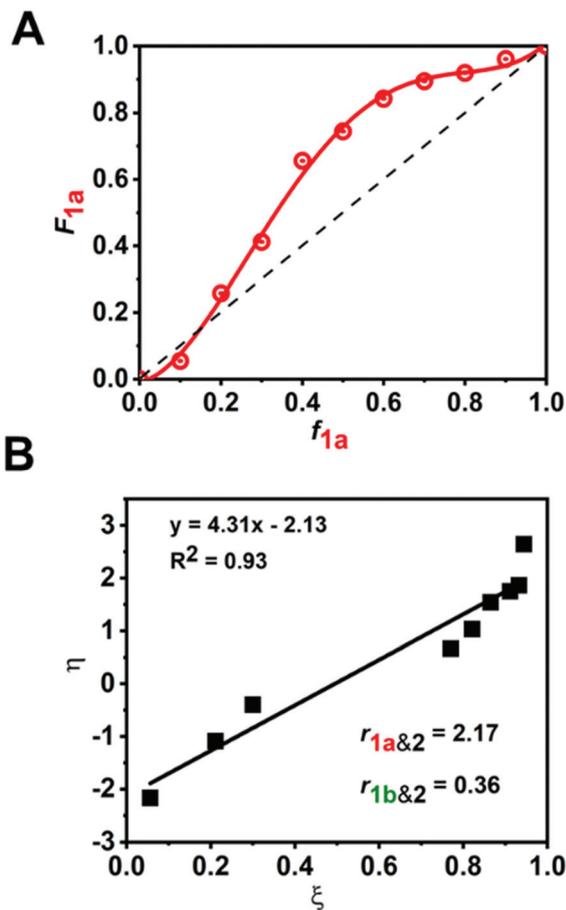
Fig. 5 (A) Lewis–Mayo plot for composition (F) of **1a** in the copolymer *vs*. feed ratio (f) of **1a**. The dashed line is an imaginary line which represents ideal copolymerization, (B) extended Kelen–Tüdős plot, given by the equation $\eta = \left(r_{\mathbf{1a}tab2} + \frac{r_{\mathbf{1b}tab2}}{\alpha}\right)\xi - \left(\frac{r_{\mathbf{1b}tab2}}{\alpha}\right)$.

reduced pressure before ^{1}H NMR analysis. To determine the degree of polymerization (DP), the polymer protons were integrated against the phenyl end group proton at δ: 7.38 ppm (2H) (see ESI Fig. S17–21†). Other protons of the phenyl end group are obscured under the solvent peak (chloroform at δ 7.28 ppm). Unfortunately at 10 min, the short oligomers formed did not precipitate with diethyl ether (Fig. S22†) and analysis of the crude mixture was required. At this time point, a DP of 5 was attained and incorporation of **1b**-*alt*-**2** was only 19%. As shown in Fig. S16,† the fraction of **1b**-*alt*-**2** strand increases gradually along the copolymer chain as the molar fraction of **1a** monomer is depleted. Combined, this evidence confirms gradient copolymer (**P5**) formation.

Effects of sequence on material properties

The thermal[1] and topological[3] properties of copolymers are highly dependent on microblock size or monomer sequence but not necessarily on their bulk composition.[23] The molar compositions and the molecular weights of all the copolymers prepared were similar. So, differences in functional properties are attributed to comonomer sequence.

Thermal properties

Material processability is dependent on the thermal properties of a copolymer. Using differential scanning calorimetry (DSC), the glass transition temperatures (T_gs) for the copolymers in bulk were determined (Fig. 6 and S23†). As expected, the uniform copolymer with propyl sidechain (**P1**) has the highest T_g whereas the polymer with an ethylene glycol sidechain (**P2**) has the lowest T_g. There was an obvious difference in T_g between the gradient copolymer (**P5**) and the diblock copolymer (**P3**). **P3** has two glass transition temperatures ($T_{g1} = -13.3$ and $T_{g2} = 26.5$ °C) which suggests that the two blocks, (**1a**-*alt*-**2**)$_{10}$ and (**1b**-*alt*-**2**)$_{10}$, act independently as two different phases. Consistent with their smaller block size, their glass transitions temperatures are lower than the measured T_g values for **P1** and **P2** of -6.9 °C and 63.0 °C, respectively. The T_g of the parent block of **1a** in **P1** is much higher than in the block copolymer **P3**. Although this partly due to reduction of chain length from 20-AB- units to 10; however, with **1b** chains having a T_g well below room temperature, it could have a plasticizing effect on the harder **1a** block and therefore lowering its T_g.[24] In contrast, **P5** has only one glass transition temperature ($T_g = 22.7$ °C) which may be attributed to the absence of interfacial separation between the multiple **1a**-*alt*-**2** and **1b**-*alt*-**2** units. Like **P5**, **P4** also has only one T_g. The single transition suggests that short block sizes of 3–4 repeating **1**-*alt*-**2** units do not induce microphase separation. Other thermal events such as melting temperature (T_m) and crystallization temperature (T_c) can be seen in thermograms of **P4** and **P5** but not present in **P3**. Thermal degradation of the polymers in bulk was assessed using thermogravimetric analysis (TGA) and derivative thermogravimetry (DTG) (Fig. S24†). None of the copolymers showed detectable weight loss up to 275 °C. These copolymers are quite stable. The least stable polymer among the five was **P1** which exhibited a maximum degradation at ~370 °C. The other copolymers, **P2**–**5** exhibited maximum degradation at ~400 °C. Since the diblock copolymer is made up of two phases we expected to see two degradation maxima. The pres-
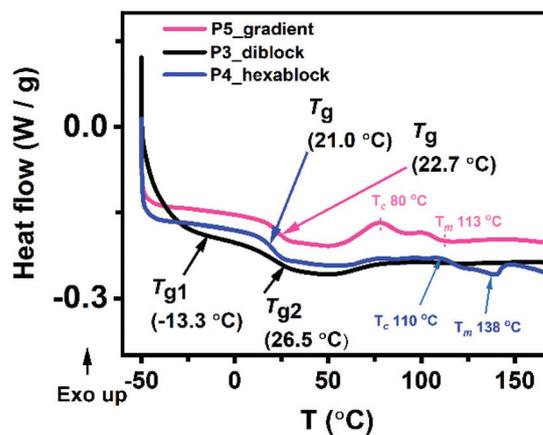

Fig. 6 (A) Differential scanning calorimetry (DSC), (B) thermogravimetric analysis (TGA) thermograms for the sequence-controlled copolymers, **P3**–**5**.

ence of a single maximum is most likely due to the close proximity of the **P1** (($1a$-*alt*-2)$_{20}$) and **P2** (($1b$-*alt*-2)$_{20}$) thermal degradation temperatures.

Topological properties

Degradation and interaction of polymeric material with other molecules such as solvents and atmospheric gases are influenced by topological features including surface wetability.[25] Here, we measured the water contact angles (WCA) for each polymer (Fig. 7 and S25†). Silicon wafers were dip-coated with

1.0% (w/w) polymer solution in chloroform and allowed to dry at ambient temperature and pressure for 48 hours. Each polymer solution was coated on three separate silicon wafers. A precise volume of water (2.5 μL) was delivered onto the polymer coated silicon wafer at a delivery speed of 1.0 μL s^{-1}. The measured contact angles of the polymer-coated substrates were consistent between replicates with only small deviations (±0.8–2.5) an indication of the reproducibility of coating. Contact angles measured for three different synthetic batches of polymers gave similar results. The contact angles on films of **P1** and **P2** were measured to establish a reference. **P1** with propyl amide side chain (**1a**) was relatively hydrophilic (CA = 79°). To our surprise, **P2** with an ethylene glycol amide side chain (**1b**) was less hydrophilic (CA = 88°) than **P1**. We believe that on a silicon matrix **P2** exposes the hydrophobic of the polymer to the air interface and therefore behaves more like a hydrophobic film.

Copolymers **P3**–**P5** displayed hydrophobicities that fall between the uniform copolymers **P1** and **P2**. Interestingly, as the number of **1b**-*alt*-**2** chain blocks within the copolymer increases, the hydrophobicity increases, as seen for hexablock **P4** and gradient **P5** copolymers. This suggests that **P3** containing only two chain blocks phase segregates more efficiently than **P4** and **P5**, exposing a hydrophilic shell to the air interface.[26]

To confirm that the surface hydrophobicity was indeed influenced by the polymer-type, we examined the surface of the polymer-coated silicon substrate by scanning electron microscopy (SEM, Fig. 8 and S26†). Measurements were done on one representative sample batch.
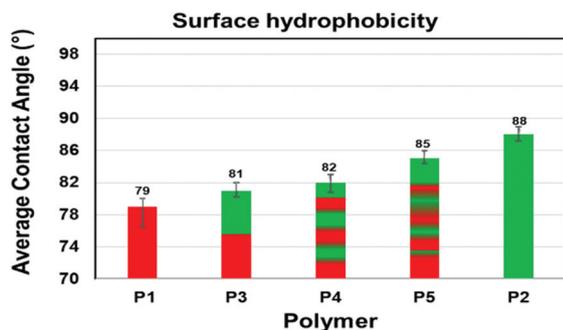

Fig. 7 Surface hydrophobicity is dependent on the sequence of **1a**-*alt*-**2** and **1b**-*alt*-**2** in the copolymer chains. Water contact angle for each polymer, from three different synthetic batches, was measured; the error bars represent the standard deviations of three measurements of the representative batch. **P1**: poly(**1a**-*alt*-**2**)$_{20}$; **P2**: poly(**1b**-*alt*-**2**)$_{20}$ shown in red and green respectively are used as reference. The contact angle for silicon wafer without polymer coat is 50° ± 2.2.
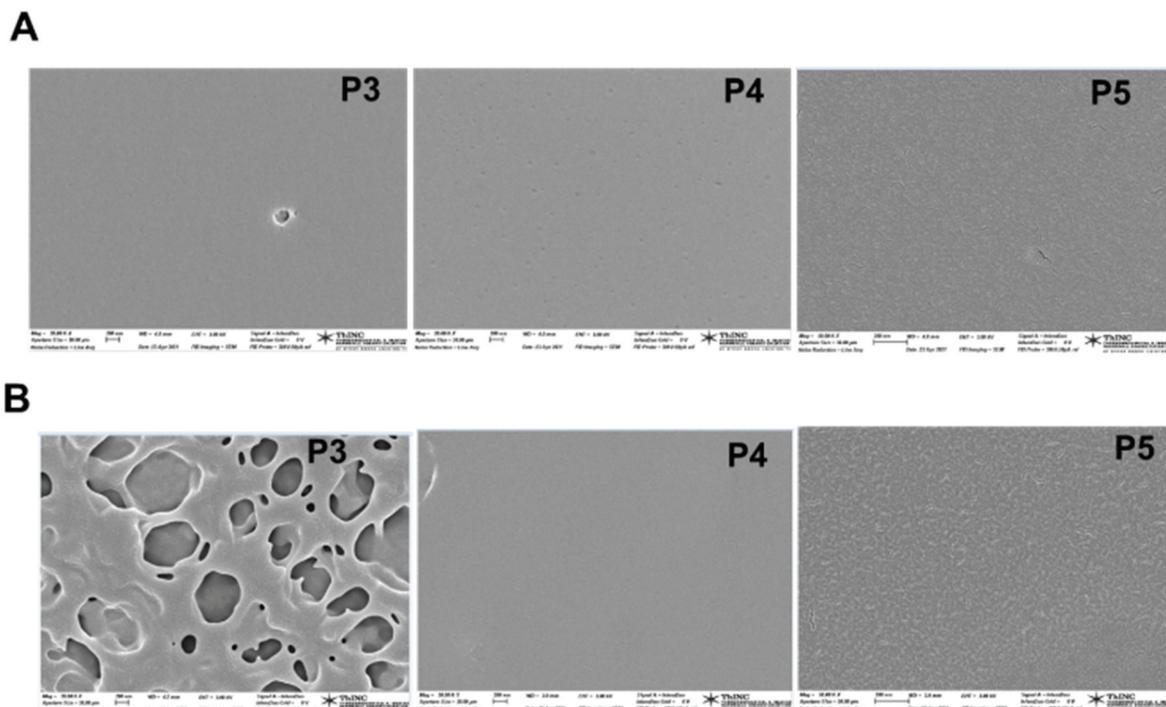

Fig. 8 SEM micrographs of films of copolymers **P1**–**P5** prepared in, (A) chloroform, (B) 2-propanol. Scale bars 200 nm.

Table 2 Water contact angle and particle size (D_H) of polymers determined by dynamic light scattering (DLS), and glass transition temperatures (T_g) of polymers P1–5

Entry	Type	T_g (°C)	Contact angle (°)	$D_{H, chloroform}$ (nm)	$D_{H, 2\text{-}propanol}$ (nm)
P1	Uniform	63.0	78.6 ± 2.5	45.1	14.6
P2	Uniform	−6.9	87.6 ± 0.6	14.1	17.8
P3	2 Blocks	−13.3, 26.5	80.9 ± 0.8	21.4	12.2
P4	6 Blocks	21.0	81.8 ± 0.8	35.0	10.8
P5	Gradient	22.7	84.7 ± 1.2	48.7	9.2

Copolymer films were prepared from chloroform or 2-propanol solutions, cast on silicon wafer substrates, and dried at ambient temperature for 48 hours. Polymer films prepared from 2-propanol solutions of **P3** exhibited distinctly hollow topological features. In contrast, films prepared from **P4** or **P5** solutions were similarly smooth. We believe that the hollow airy features seen in **P3** are dominated by the **1a**-*alt*-**2** block. The diblock copolymer most likely phase-separates efficiently as its **1b**-*alt*-**2** block strongly adheres to the silicon surface due to intermolecular H-bond interactions and exposes the **1a**-*alt*-**2** block to the air interface. SEM images of **P1** cast from 2-propanol (Fig. S26B†) also form films that trap air-bubbles at the air interface.

Using dynamic light scattering (DLS), we explored the particle size of the copolymers in chloroform and 2-propanol (Fig. S27 and 28,† Table 2). The particle size was dependent on polymer type as well as the solvent. In general, copolymers formed smaller particles in the more polar solvent (2-propanol) than in the less polar solvent (chloroform). The size of the **P2** particle with ethylene glycol side chain is bigger in 2-propanol than in chloroform. In contrast, **P1** with propyl side chain is bigger in chloroform than in 2-propanol. Due to the presence of the ethylene glycol system in **P2**, intermolecular interaction through hydrogen-bonding with 2-propanol can result in higher solvation, and therefore swelling. The particle sizes of the sequence-defined copolymers increase or decrease based on the distribution **1b**-*alt*-**2** strand in the copolymer chains. For instance, particle size of diblock copolymer **P3** is larger than hexablock **P4** and gradient copolymer **P5** in 2-propanol but smaller in chloroform. This solvent dependent particle size behavior of the sequence-defined copolymers suggests that the diblock copolymer strongly phase segregates than the hexablock and gradient copolymers.

Conclusion

In this work, we demonstrate that AROMP is a versatile method to prepare a myriad of polymeric materials with molecularly defined structures whose surface and thermal properties can be tuned. A three-monomer system **1a**/**1b**/**2** was utilized to prepare a gradient copolymer which had thermal and morphological properties similar to copolymer with hexablock units but different than that of the diblock copolymer. This work in addition to current works[17,27,28] suggest that with the choice of monomers with suitable reactivities, laborious multi-step synthetic routes could be bypassed while still achieving copolymers with multiblock segments in a one-pot approach.

Therefore, gradient copolymer preparation with AROMP presents an opportunity to synthesize variable sequence copolymers with a wider variety of possibilities than traditional norbornene-ROMP.

There are additional prospects to tune copolymer flexibility by varying spacer length,[29] and to prepare degradable copolymers[18] through appropriate selection of the unstrained cyclic alkene in place of monomer **2**.

Experimental section

Materials and general methods

All air-sensitive and metathesis reactions were performed under N_2 by means of standard Schlenk or glove box techniques. Polystyrene standards and $Cl_2(H_2IMes)(PCy_3)$ Ru=CHPh (Grubbs 2nd generation catalyst) were purchased from Aldrich. Grubbs 3rd generation catalyst $(3\text{-}BrPyr)_2Cl_2(H_2IMes)Ru$=CHPh, **3**, was prepared from 2nd generation catalyst and 3-bromopyridine.[30] Dry, oxygen-free CH_2Cl_2, was obtained with a Pure Process Technology solvent purification system. Mallinckrodt silica gel-60 (230–400 mesh) was used for column chromatography. Analytical thin-layer chromatography was performed on precoated silica gel plates (60F254), and Combi-Flash chromatography on RediSep normal-phase silica columns (silica gel-60, 230–400 mesh). Bruker Nanobay 400, AVANCE III 500 MHz, and AVANCE III 700 MHz instruments were used for NMR spectroscopy.

Gel permeation chromatography/size exclusion chromatography

Analyses were performed on a system composed of Shimadzu SCL-10A controller, a Shimadzu LC-20AT pump, and a Shimadzu CTO-10AS column oven equipped with combined Phenogel columns: 5 μm linear (2) (300 × 7.8 mm, 100–10 000k) and 5 μm 50 Å (300 × 7.8 mm, 100–3k), and coupled with a Brookhaven Instruments BI-DNDC refractometer. The mobile phase used was HPLC-grade tetrahydrofuran (filtered with 0.2 μL PTFE filter) at 30 °C and 0.7 mL min^{-1}. High resolution mass spectra were recorded on an Agilent 1260 LC/G6224 qTOF instrument.

Water contact angle

1% (w/w) polymer solutions were prepared in chloroform. Silicon wafers were dip-coated with the polymer solutions and dried at ambient temperature and pressure for 48 h. The water contact angles were measured with Data Physics instrument's optical contact angle goniometers and drop shape analysis systems and SCA 20 software in sessile drop mode. Each measurement was performed on three dip-coated wafers for each polymer sample; the average and standard deviations were taken.

Thermal analysis

Solid polymer samples were used. The experiments were performed on a TA Instruments Q2000 differential scanning calorimeter with Wizard software (TA Instruments Q Series software). Heat flow (Tzero) calibration was performed with sapphire standards, and the temperature (cell constant) was calibrated using indium at a scan rate of 10 °C min^{-1}. All differential scanning calorimetry was performed with a DSC Q2000 V24.11 Build 124 Module DSC Standard Cell RC under a N$_2$ flow (50 mL min^{-1}) using S5 Tzero aluminum pans and hermetic lids. The sample weights ranged from 5 to 8 mg. The samples were first equilibrated at −50 °C and then heated to 200 °C at 5 °C min^{-1}. Thermogravimetric analysis was performed with a TGA Q50 V20.13 Build 39 equipped with a platinum pan. The sample sizes ranged from 6 to 12 mg. Weight loss data were collected from 30 to 600 °C at 5 °C min^{-1} under a N$_2$ flow (60 mL min^{-1}).

Scanning electron microscopy (SEM)

Samples were analyzed using the SEISS Crossbeam 340 focus ion beam-scanning electron microscope (FIB-SEM) at 30 kV. Polymer films were prepared by dip-coating a silicon substrate with 1% (w/w) polymer solution in chloroform or 2-propanol and dried under vacuum. Samples were analyzed without staining.

Dynamic light scattering (DLS)

Samples were analyzed on a 90 Plus Particle Size Analyzer (Brookhaven Instruments), a 35 mW red diode laser with a wavelength of 659.0 nm, scattering angle 90, 25 °C. Each signal was recorded for 60 s, and the signals for 5 consecutive runs were averaged. 1% (w/w) polymer solutions were prepared in the desired solvent, filtered using 0.2 μm PTFE membrane, and 200 μL solution transferred into a cuvette.

Monomer and polymer preparation

1b: 500 mg bicyclo[4.2.0]oct-6-ene-7-carboxylic acid (3.29 mmol, 1 eq.) and 633 mg EDC·HCl (3.3 mmol, 1 eq.) were dissolved in 15 ml CH$_2$Cl$_2$. Diisopropylethylamine (1.15 ml, 6.58 mmol, 2 eq.) and *N*-2-(2-ethoxyethoxy)ethan-1-amine (0.48 ml, 3.29 mmol, 1 eq.) were added to the mixture. The reaction was stirred for 3 h at 23 °C. The mixture was diluted with 100 mL CH$_2$Cl$_2$ and then sequentially washed with 1 N HCl (25 mL), sat. NaHCO$_3$ (25 mL), DI H$_2$O (25 mL). Flash chromatography on silica gel using 20% acetone in CH$_2$Cl$_2$ ($R_f \approx 0.45$) afforded the desired product as colorless viscous oil in 52% (459 mg) isolated yield. ^{1}H NMR (500 MHz, CDCl$_3$) δ ppm 5.93 (s, 1H), 3.64–3.61 (m, 2H), 3.61–3.58 (m, 4H), 3.54 (q, 2H, J = 6.95 Hz), 3.54–3.50 (m, 2H), 2.88 (d, 1H, J = 14.0 Hz), 2.69 (dt, 1H, J = 12.0, 3.71 Hz), 2.35 (m, 1H), 2.20 (d, 1H, J = 12.3 Hz), 2.13 = 2.05 (m, 2H), 1.91 (m, 1H), 1.75 (m, 1H), 1.32 (m, 2H), 1.23 (t, 3H, J = 6.93 Hz), 1.12 (m, 1H). ^{13}C NMR (500 MHz, CDCl$_3$, δ) 164.4, 161.5, 126.8, 70.5, 70.2, 69.9, 66.9, 38.7, 38.0, 34.1, 33.1, 27.4, 26.9, 24.9, 15.4. HRMS: *m*/*z* calc 268.1907; found 268.1906 [M + H]$^+$.

P1: poly(**1a**-*alt*-**2**)$_{20}$: A solution of **1a** (90 mg, 0.47 mmol) in dichloromethane (1000 μL) and a solution of **3** (20.5 mg, 0.023 mmol) in dichloromethane (500 μL) were mixed in a septum capped vial previously sparged with nitrogen. The mixture was incubated at 40 °C for 15 min. Monomer **2** (94 μL, 76.1 mg, 0.927 mmol) was added and after 80 min, the reaction was terminated with ethyl vinyl ether (100 μL). Polymer was precipitated in diethyl ether and dried under vacuum to yield the copolymer as off-white sponge-like solid (75% isolated yield).

P2: poly(**1b**-*alt*-**2**)$_{20}$: A solution of **1b** (100 mg, 0.37 mmol) in dichloromethane (1100 μL) and a solution of **3** (16.5 mg, 0.019 mmol) in dichloromethane (400 μL) were mixed in a septum capped vial previously sparged with nitrogen. The mixture was incubated at 40 °C for 15 min. Monomer **2** (93 μL, 75.6 mg, 0.92 mmol) was added and after 180 min, reaction was terminated with ethyl vinyl ether (100 μL). Polymer was precipitated in diethyl ether and dried under vacuum to yield the copolymer as off-white very viscous liquid-solid-like material (66% isolated yield).

P3: diblock, poly(**1a**-*alt*-**2**)$_{10}$-*b*-(**1b**-*alt*-**2**)$_{10}$: A solution of **3** (23 mg, 0.026 mmol) in dichloromethane (550 μL) and a solution of **1a** (50 mg, 0.26 mmol, 10 eq.) in dichloromethane (600 μL) were mixed in a septum capped vial previously sparged with nitrogen. The mixture was incubated at 40 °C for 15 min. Monomer **2** (66 μL, 53.2 mg, 0.65 mmol, 25 eq.) was added in excess. The reaction was allowed to proceed for an additional 40 min and then a solution of **1b** (69.2 mg, 0.26 mmol) in dichloromethane (700 μL) was added. After an additional 140 min, the reaction was terminated with ethyl vinyl ether (100 μL). Polymer was precipitated in diethyl ether and dried under vacuum to yield the copolymer as off-white solid (74% isolated yield).

P4: hexablock, poly[(**1a**-*alt*-**2**)-*b*-(**1b**-*alt*-**2**)]$_{n=4, 3, 3}$: A solution of **3** (23 mg, 0.026 mmol) in dichloromethane (400 μL) and a solution of **1a** (20 mg, 0.103 mmol, 4 eq.) in dichloromethane (200 μL) were mixed in a septum capped vial previously sparged with nitrogen. *Step 1*: after the mixture had been incubated at 40 °C for 15 min, monomer **2** was added in excess (79 μL, 63.8 mg, 0.78 mmol, 30 eq.) and the reaction allowed to proceed for an additional 25 min. *Step 2*: a solution of **1b** (27.5 mg, 0.103 mmol, 4 eq.) in dichloromethane (250 μL) was added to the mixture from step 1 and the reaction allowed to continue for an additional 35 min. *Step 3*: a solution of **1a** (15 mg, 0.078 mmol, 3 eq.) in dichloromethane (151 μL) was added to the step 2 mixture and the reaction allowed to continue for an additional 25 min. *Step 4*: a solution of **1b** (20.6 mg, 0.077 mmol, 3 eq.) in dichloromethane (187 μL) was added to the step 3 mixture and the reaction allowed to continue for an additional 35 min. *Steps 3* and *4* were repeated in sequence and the reaction was terminated with ethyl vinyl ether (500 μL). Polymer was precipitated in diethyl ether and dried under vacuum to yield the copolymer as off-white solid (78% isolated yield).

P5: gradient, poly(**1a**-*alt*-**2**)$_{10}$-*grad*-(**1b**-*alt*-**2**)$_{10}$: A solution of **3** (22.9 mg, 0.026 mmol) in dichloromethane (550 μL) and a

solution of **1a** (50 mg, 0.26 mmol) in dichloromethane (600 μL) were mixed. The mixture was incubated at 40 °C for 15 min, followed by addition of a solution of **1b** (69.2 mg, 0.26 mmol) in dichloromethane (700 μL) and **2** (53 μL, 42.6 mg, 0.52 mmol). After 180 min, the reaction was terminated with ethyl vinyl ether (100 μL). Polymer was precipitated in diethyl ether and dried under vacuum to yield the copolymer as off-white solid (65% isolated yield).

ROM kinetics of 1a. A solution of **3** (114.4 mg, 0.129 mmol) in dichloromethane (500 μL) was added to a septum capped NMR tube. Reaction at time t = 0 min was recorded by ^{1}H-NMR spectroscopy at 40 °C. A solution of **1a** in dichloromethane (25 mg, 0.129 mmol, 360 μL) was added quickly into the NMR tube and mixed. Reaction was carried on at 40 °C and at specified time intervals, ^{1}H-NMR spectra were acquired. Data were plotted as concentration *vs.* time and fitted with the best rate law equation.

ROM kinetics of 1b. A solution of **3** (114.4 mg, 0.129 mmol) in dichloromethane (500 μL) was added to a septum capped NMR tube. Reaction at time t = 0 min was recorded by ^{1}H-NMR spectroscopy at 40 °C. A solution of **1b** in dichloromethane (34.5 mg, 0.129 mmol, 330 μL) was added quickly into the NMR tube and mixed. Reaction was carried on at 40 °C and at specified time intervals, ^{1}H-NMR spectra were acquired. Data were plotted as concentration *vs.* time and fitted with best rate law equation.

Author contributions

Francis Boadi: conceptualization, validation, investigation, writing-original draft, writing-review and editing. Nicole S. Sampson: conceptualization, writing-review and editing, resources, supervision, project administration.

Conflicts of interest

There are no conflicts to declare.

Acknowledgements

Notes and references

1 E. A. Hoff, G. X. De Hoe, C. M. Mulvaney, M. A. Hillmyer and C. A. Alabi, *J. Am. Chem. Soc.*, 2020, **142**, 6729–6736.
2 W. Jakubowski, A. Juhari, A. Best, K. Koynov, T. Pakula and K. Matyjaszewski, *Polymer*, 2008, **49**, 1567–1578.
3 G. Li and N. S. Sampson, *Macromolecules*, 2018, **51**, 3932–3940.
4 W. Yuan, M. M. Mok, J. Kim, C. L. H. Wong, C. M. Dettmer, S. T. Nguyen, J. M. Torkelson and K. R. Shull, *Langmuir*, 2010, **26**, 3261–3267.
5 J. Kim, H. Zhou, S. T. Nguyen and J. M. Torkelson, *Polymer*, 2006, **47**, 5799–5809.
6 J. Kim, M. M. Mok, R. W. Sandoval, D. J. Woo and J. M. Torkelson, *Macromolecules*, 2006, **39**, 6152–6160.
7 X. Guo, T. Zhang, Y. Wu, W. Shi, B. Choi, A. Feng and S. H. Thang, *Polym. Chem.*, 2020, **11**, 6794–6802.
8 Z. Wang, T. Liu, Y. Zhao, J. Lee, Q. Wei, J. Yan, S. Li, M. Olszewski, R. Yin, Y. Zhai, M. R. Bockstaller and K. Matyjaszewski, *Macromolecules*, 2019, **52**, 9466–9475.
9 O. Sedlacek, K. Lava, B. Verbraeken, S. Kasmi, B. G. De Geest and R. Hoogenboom, *J. Am. Chem. Soc.*, 2019, **141**, 9617–9622.
10 K. Matyjaszewski, *Macromolecules*, 1993, **26**, 1787–1788.
11 C. W. Bielawski and R. H. Grubbs, *Prog. Polym. Sci.*, 2007, **32**, 1–29.
12 C. M. Dettmer, M. K. Gray, J. M. Torkelson and S. T. Nguyen, *Macromolecules*, 2004, **37**, 5504–5512.
13 A. B. Chang, T.-P. Lin, N. B. Thompson, S.-X. Luo, A. L. Liberman-Martin, H.-Y. Chen, B. Lee and R. H. Grubbs, *J. Am. Chem. Soc.*, 2017, **139**, 17683–17693.
14 T.-P. Lin, A. B. Chang, H.-Y. Chen, A. L. Liberman-Martin, C. M. Bates, M. J. Voegtle, C. A. Bauer and R. H. Grubbs, *J. Am. Chem. Soc.*, 2017, **139**, 3896–3903.
15 L. Jiang, D. Nykypanchuk, A. E. Ribbe and J. Rzayev, *ACS Macro Lett.*, 2018, **7**, 619–623.
16 H. Yuan, T. Kida, R. Tanaka, Z. Cai, Y. Nakayama and T. Shiono, *Polym. Chem.*, 2021, **12**, 189–195.
17 S. Pal, M. Alizadeh, P. Kong and A. F. M. Kilbinger, *Chem. Sci.*, 2021, **12**, 6705–6711.
18 F. O. Boadi, J. Zhang, X. Yu, S. R. Bhatia and N. S. Sampson, *Macromolecules*, 2020, **53**, 5857–5868.
19 J. Engelke, J. Brandt, C. Barner-Kowollik and A. Lederer, *Polym. Chem.*, 2019, **10**, 3410–3425.
20 F. Tüdos, T. Kelen, T. Földes-bereznich and B. Turcsányi, *J. Macromol. Sci., Part A*, 1976, **10**, 1513–1540.
21 T. Gleede, J. C. Markwart, N. Huber, E. Rieger and F. R. Wurm, *Macromolecules*, 2019, **52**, 9703–9714.
22 A. S. Brar, Sunita and C. V. V. Satyanarayana, *Polym. J.*, 1992, **24**, 879–887.
23 K. Matyjaszewski, *Science*, 2011, **333**, 1104–1105.
24 A. B. Kutikov and J. Song, *ACS Biomater. Sci. Eng.*, 2015, **1**, 463–480.
25 N. J. Shirtcliffe, G. McHale and M. I. Newton, *J. Polym. Sci., Part B: Polym. Phys.*, 2011, **49**, 1203–1217.
26 S. K. Filippov, B. Verbraeken, P. V. Konarev, D. I. Svergun, B. Angelov, N. S. Vishnevetskaya, C. M. Papadakis,

S. Rogers, A. Radulescu, T. Courtin, J. C. Martins, L. Starovoytova, M. Hruby, P. Stepanek, V. S. Kravchenko, I. I. Potemkin and R. Hoogenboom, *J. Phys. Chem. Lett.*, 2017, **8**, 3800–3804.

27 M. Yasir, P. Liu, J. C. Markwart, O. Suraeva, F. R. Wurm, J. Smart, M. Lattuada and A. F. M. Kilbinger, *Angew. Chem.*, 2020, **59**, 13597–13601.

28 C. Wahlen, J. Blankenburg, P. von Tiedemann, J. Ewald, P. Sajkiewicz, A. H. E. Müller, G. Floudas and H. Frey, *Macromolecules*, 2020, **53**, 10397–10408.

29 J. Zhang, G. Li and N. S. Sampson, *ACS Macro Lett.*, 2018, **7**, 1068–1072.

30 J. A. Love, J. P. Morgan, T. M. Trnka and R. H. Grubbs, *Angew. Chem., Int. Ed.*, 2002, **41**, 4035–4037.